[Z(I Imaging Corporation, Englewood, CO)] with pixel size of 0.4 nm on the sample. Shadowed specimens were prepared as described (*2*). Handedness of the shadowed specimen was determined using the 5.1-nm left-handed actin repeat and the 37.5-nm right-handed half-twist crossover repeat, both visible in the images (Fig. 2D).

11. Image processing of single particles of *Acanthamoeba* Arp2/3 complex. Interactive selection from 46 images yielded 4414 particles (Fig. 1A). The particles were processed and analyzed using the EMAN (*28*) and COAN (*29*) software packages. A correction for the contrast transfer function was applied for all images. Absolute scaling was performed using the known helical symmetry of actin filaments present in the same images. For 3D reconstruction, particles were aligned to each other using the reference-free method, classified into 20 to 25 classes, and averaged. Briefly, particles that appear to be similar (by dot product) to one another were grouped together into a predefined number of groups, and then the particles within each group were mutually aligned and averaged. This generated a class average for each group that should represent one characteristic view of the particle. Several of these averages were then selected manually and passed to a Fourier common-lines routine that determines the relative orientations (Euler angles) of all selected averages, which are then combined to calculate an initial 3D model. This initial model was then iteratively refined against the data. Convergence was achieved when the Fourier shell correlation between successive iterations stabilized. Three independent starting models were generated from different subsets of the *Acanthamoeba* data set. Several rounds (15 to 25) of refinement were performed for each of these models using the complete data set. The three calculations converged to the same structure (Fig. 1D), as suggested by the high correlation values.
12. B. Böttcher, S. A. Wynne, R. A. Crowther, *Nature* **386**, 88 (1997).
13. Scar WA-Cys, containing a single cysteine residue at its $NH_2$-terminus, was purified as described (*22*) and then reacted with equimolar monoamino Nanogold (Nanoprobes) in 100 mM NaCl and 10 mM $NaPO_4$ (pH 7.0) for 16 hours at 4°C. Nanogold-labeled WA was further purified by S-100 gel filtration chromatography in 100 mM NaCl, 10 mM Tris-HCl (pH 8.0), and 2 mM DTT. Images of frozen-hydrated Arp2/3 complex labeled with nanogold-labeled WA were recorded in focal pairs at 0.5 and 2.5 μm defocus using low-dose conditions. The position of the gold label within the reconstruction was calculated by backprojection from 10 class averages of gold-decorated particles (generated by superposition of the focal-pair images) after alignment to projections calculated from the undecorated reconstruction.
14. The budding yeast *Saccharomyces cerevisiae* Arp2/3 complex was purified as described (*30*). Bee1-WA, the 125 COOH-terminal residues of yeast Beep1 was purified as described (*31, 32*). Phalloidin-stabilized actin filaments were incubated with 25 nM Arp2/3 complex and 50 nM Bee1-WA domain in UBA buffer [50 mM Hepes (pH 7.5), 100 mM KCl, 3 mM $MgCl_2$, 1 mM EGTA, 0.2 mM ATP] for 5 min at 22°C. The pellet containing actin filaments and attached complexes was resuspended in UBA buffer and applied to copper grids coated with triafol holey carbon films (pelleting: Beckman-Coulter TLA-100 rotor at 70,000 rpm for 10 min at 4°C). The samples were stained with aqueous uranyl acetate, air-dried, and imaged at 2 μm defocus. The yeast data set consisted of 1157 particles selected from 13 images, and was processed following the procedure described for *Acanthamoeba* (*11*), which yielded a reconstruction very similar to that of *Acanthamoeba* (Fig. 1D).
15. R. D. Mullins, W. F. Stafford, T. D. Pollard, *J. Cell Biol.* **136**, 331 (1997).
16. Actin was isolated from rabbit skeletal muscle acetone powder (*33*) and further purified by gel filtration on Sephacryl S-300 in Ca-G buffer (*22*). Branches were prepared by polymerizing 4 μM Mg-ATP actin in the presence of 50 nM Arp2/3 and 200 nM Scar WA in Mg-G buffer [2 mM imidazole (pH 7.0), 200 μM ATP, 100 μM $MgCl_2$, 500 μM DTT] containing 1× KMEI [50 mM KCl, 100 μM $MgCl_2$, 1 mM EGTA, 10 mM imidazole (pH 7.0)] for 2 min at 22°C followed by addition of 4 μM phalloidin 1 min before application to the Quantifoil grids. For the reconstruction of the branch junction, 167 clearly visible branches were interactively selected from 127 images. A reference-free alignment of these images gave class averages with branch angles of ~70°. The class with the clearest definition of actin monomers in the filaments was selected for reference-based alignment. To overcome the blurring of details due to small differences in branching angles, we generated three references emphasizing different portions of the structure. One reference focused on the mother filament, one on the daughter filament, and one on the central density of the branch junction. The complete data set was aligned to each of the references. Independent 2D averages were calculated and then merged (Fig. 2B). Atomic models of actin filaments (*19*) were fitted to the projection density of the mother and daughter filaments using COAN (*29*).
17. For myosin decoration, actin filaments were polymerized in the presence of Arp2/3 complex (25 nM) and Bee1-WA domain (50 nM) in UBA buffer (*32*). Samples were applied to the triafol grids and incubated with expressed smooth muscle myosin catalytic domain (no light chains) (*34*) prior to staining.
18. T. M. Svitkina, A. B. Verkhovsky, K. M. McQuade, G. G. Borisy, *J. Cell Biol.* **139**, 397 (1997).
19. M. Lorenz, D. Popp, K. C. Holmes, *J. Mol. Biol.* **234**, 826 (1993).
20. H. N. Higgs, T. D. Pollard, *J. Biol. Chem.* **274**, 32531 (1999).
21. D. C. Winter, E. Y. Choe, R. Li, *Proc. Natl. Acad. Sci. U.S.A.* **96**, 7288 (1999).
22. K. J. Amann, T. D. Pollard, *Nature Cell Biol.* **3**, 306 (2001).
23. D. Pantaloni, R. Boujemaa, D. Didry, P. Gounon, M. F. Carlier, *Nature Cell Biol.* **2**, 385 (2000).
24. L. M. Machesky, R. H. Insall, *Curr. Biol.* **8**, 1347 (1998).
25. L. Blanchoin *et al.*, *Nature* **404**, 1007 (2000).
26. L. M. Machesky, S. J. Atkinson, C. Ampe, J. Vandekerckhove, T. D. Pollard, *J. Cell Biol.* **127**, 107 (1994).
27. M. Way, J. Gooch, B. Pope, A. G. Weeds, *J. Cell Biol.* **109**, 593 (1989).
28. S. J. Ludtke, P. R. Baldwin, W. Chiu, *J. Struct. Biol.* **128**, 82 (1999).
29. N. Volkmann, D. Hanein, *J. Struct. Biol.* **125**, 176 (1999).
30. D. Winter, A. V. Podtelejnikov, M. Mann, R. Li, *Curr. Biol.* **7**, 519 (1997).
31. R. Li, *J. Cell Biol.* **136**, 649 (1997).
32. D. Winter, T. Lechler, R. Li, *Curr. Biol.* **9**, 501 (1999).
33. J. A. Spudich, S. Watt, *J. Biol. Chem.* **246**, 4866 (1971).
34. K. M. Trybus, *J. Biol. Chem.* **269**, 20819 (1994).

35. We are grateful to G. Ouyang for technical assistance, to K. M. Trybus and S. Lowey for the myosin sample, to S. Almo for critical reading of the manuscript, and to R. Liddington for helpful discussions and valuable comments on the manuscript. Supported by NIH research grants (T.D.P., R.L.), an NIH postdoctoral fellowship (K.J.A.), and the Human Frontier Science Program (C.E.). D.H. is a Pew Scholar in the Biomedical Sciences.

31 May 2001; accepted 24 July 2001
Published online 30 August 2001;
10.1126/science.1063025
Include this information when citing this paper.

# *Trans*-Suppression of Misfolding in an Amyloid Disease

**Per Hammarström, Frank Schneider, Jeffery W. Kelly***

**The transthyretin (TTR) amyloid diseases, representative of numerous misfolding disorders, are of considerable interest because there are mutations that cause or suppress disease. The $Val^{30} \rightarrow Met^{30}$ (V30M) TTR mutation is the most prevalent cause of familial amyloid polyneuropathy in heterozygotes, whereas a $Thr^{119} \rightarrow Met^{119}$ (T119M) mutation on the second TTR allele protects V30M carriers from disease. Here, we show that the incorporation of one or more T119M TTR subunits into a predominantly V30M tetramer strongly stabilized the mixed tetramer against dissociation. Dissociation is required for amyloid formation, so these findings provide a molecular explanation for intragenic *trans*-suppression of amyloidosis. The data also suggest a potential therapeutic strategy, provide insight into tissue-specific deposition and amyloid composition, and support the validity of the amyloid hypothesis in human disease.**

The amyloidoses are a large group of protein misfolding diseases (*1–3*). The 80 transthyretin (TTR) amyloid diseases are representative of those where a full-length protein composes the fibrils. The TTR familial amyloid polyneuropathy (FAP) mutations (e.g., V30M) make TTR more susceptible to dissociation and the conformational changes that enable amyloid deposition and pathology. Compound heterozygotes having V30M and T119M TTR mutations on different alleles have few, if any, manifestations of FAP (*4, 5*), suggesting that the incorporation of a stabilizing subunit in an oligomeric protein such as TTR can protect against misfolding and disease. Previous studies document the increased stability of T119M-containing TTR and the decreased stability of the V30M-containing TTR, relative to the wild type (WT) (*6–8*).

Here, we evaluate the amyloidogenicity and stability of individual tetramers with defined V30M and/or T119M subunit composition to explain the T119M *trans*-suppression that protects compound heterozygotes from disease.

Department of Chemistry and The Skaggs Institute of Chemical Biology, The Scripps Research Institute, 10550 North Torrey Pines Road BCC265, La Jolla, CA 92037, USA.

*To whom correspondence should be addressed. E-mail: jkelly@scripps.edu

The V30M/T119M TTR hybrid tetramers were synthesized by double transformation and coexpression in *E. coli*. An anionic tandem FLAG tag ($FT_2$) sequence $(DYKDDDDK)_2$ (*9*) was added to the $NH_2$-terminus of T119M TTR to facilitate ion exchange separation of tetramers having different numbers of T119M subunits (nondenaturing conditions; Fig. 1A). The greater the number of $FT_2$-T119M subunits in the TTR tetramer, the longer the retention time. Reverse-phase high-pressure liquid chromatography (RP-HPLC) (Fig. 1B) (denaturing conditions) and SDS–polyacrylamide gel electrophoresis (*10*) analysis of individual peaks collected from a preparative anion exchange separation revealed that tetramers **1**, **2**, **3**, **4**, and **5** contained zero, one, two, three, and four $FT_2$-T119M subunits, respectively, with the balance being V30M. Tetramers **2** to **5** dissociate very slowly at 37°C (no exchange after 5 days), allowing studies on tetramers **1** through **5** to be carried out without complications from post-separation subunit exchange (*11*). Appending the $FT_2$ sequence to the $NH_2$-terminus of WT TTR does not alter its stability, rate of subunit self-exchange, or pH-dependent amyloidogenicity (*11*). Isolated tetramers composed of WT and/or T119M, and WT and/or V30M subunits, were prepared analogously.

Because partial acid denaturation (endocytic pathway) has been implicated in fibril formation for several amyloid proteins (*1*), we evaluated the pH-dependent solubility of tetramers **1** to **5**. The V30M homotetramer **1** and tetramer **2** precipitated over a pH range of 4.8 to 4.0. However, tetramer **2** incorporating a single $FT_2$-T119M subunit exhibited significantly reduced deposition (*10*). The inclusion of two or more suppressor subunits rendered tetramers **3**, **4**, and **5** soluble from pH 7 to 3. The amyloidogenicity of hybrid tetramers **2**, **3**, and **4** was evaluated at pH 4.4 (the pH maximum of V30M fibril formation from homotetramer **1**) by both turbidity and thioflavin T binding. Substituting V30M subunits with $FT_2$-T119M subunits in the TTR tetramer caused a stoichiometry-dependent inhibition of fibril formation (Fig. 2A). The inclusion of one suppressor subunit (tetramer **2**) reduced amyloidogenicity by 50%, whereas the presence of two or more suppressor subunits (e.g., tetramer **3**, **4**, or **5**) reduced amyloidogenicity by more than 90% at physiological TTR concentrations (at 37°C). Comparing tetramers **1** through **5** from compound heterozygotes to V30M/$FT_2$-WT tetramer **1** and tetramers **6** to **9** (found in heterozygous FAP patients) revealed that the WT subunits are poor amyloid fibril suppressors (Fig. 2, A and B). WT TTR amyloidogenesis (pH 4.4) was inhibited by 45 and 80% by the incorporation of one and two $FT_2$-T119M subunits, respectively (tetramers **11** and **12**; Fig. 2C), suggesting generality.

The influence of suppressor subunit stoichiometry on tetramer stability was evaluated by the guanidinium thiocyanate (GdmSCN)–mediated transition from folded tetramer to unfolded monomers (Fig. 3A). GdmSCN denaturation exhibits hysteresis due to anion stabilization of the tetramer—ideal for this application, because it prevents reequilibration of hybrid tetramer subunit stoichiometry during measurements (*12*). Stability differences can be detected by comparing denaturant curve midpoints ($\Delta c_{1/2}$), whereas changes in the free energy of unfolding ($\Delta\Delta G_{NU}$) can be estimated by the linear extrapolation method (imperfect due to hysteresis) (*13*). Tetramer stability increased in a nonlinear fashion with T119M subunit stoichiometry, and the $\Delta c_{1/2}$ between homotetramers **1** and **5** was 0.36 M, with $\Delta\Delta G_{NU} \approx 1.8$ kcal/mol (*10*). The *trans*-suppression effect is similar in magnitude to the *cis*-global suppressor mutations that prevent P22 tailspike (*14*) and P53 tumor suppressor (*15*) misfolding. Furthermore, subunit exchange experiments show that homotetrameric T119M TTR self-exchanges subunits >100-fold slower than both WT and V30M TTR, likely owing to the differential stabilization of the tetramer relative to the transition state for dissociation (Fig. 3C). Thus, the T119M stabilization of the tetramer in combination with the high kinetic barriers for dissociation rationalize the mechanistic basis for intragenic *trans*-suppression. In comparison, increasing the WT stoichiometry relative to V30M revealed a modest stability increase [$\Delta c_{1/2}$ = 0.10 M; $\Delta\Delta G_{NU} \approx 0.5$ kcal/mol (*10*)] and similar subunit self-exchange rates (Fig. 3, B and C). Tetramer **1** and tetramers **6** to **9** also exhibited very similar amyloidogenicity at pH 4.4 (Fig. 2B), suggesting similar stability toward acid denaturation, consistent with epidemiology results showing no major differences in FAP pathology or age of onset when comparing V30M homozygotes to heterozygotes (*16*–*19*).

Mixing equimolar amounts of $FT_2$-T119M homotetramers (or T119M homotetramers) with V30M homotetramers under conditions precluding exchange had no effect on V30M fibril formation (Fig. 4, A and B), suggesting that the stabilizing effect of T119M requires subunit exchange. Hybrid tetramers formed by a modest extent of subunit exchange (Fig. 4C) inhibited amyloidosis by 20% (*20*), whereas a near-statistical mixture of tetramers created by reconstitution of unfolded V30M and T119M monomers (*20*) inhibited amyloid formation by 70% (Fig. 4E). The extent of subunit mixing determined the extent of amyloid inhibition observed (Fig. 4, A through E).

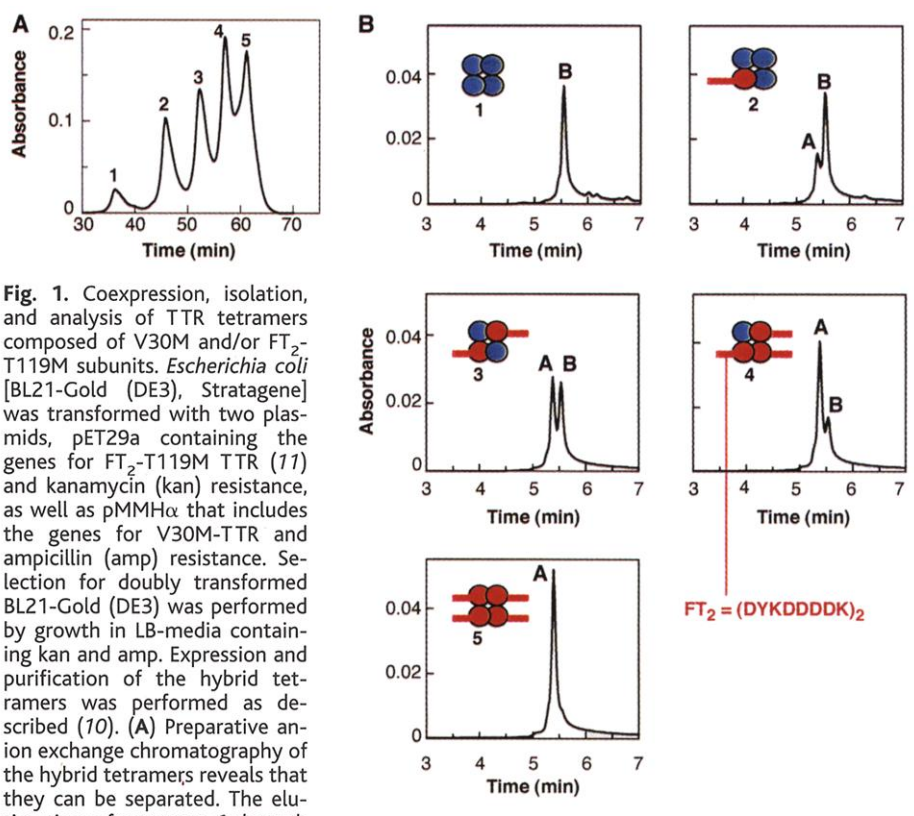


**Fig. 1.** Coexpression, isolation, and analysis of TTR tetramers composed of V30M and/or $FT_2$-T119M subunits. *Escherichia coli* [BL21-Gold (DE3), Stratagene] was transformed with two plasmids, pET29a containing the genes for $FT_2$-T119M TTR (*11*) and kanamycin (kan) resistance, as well as pMMHα that includes the genes for V30M-TTR and ampicillin (amp) resistance. Selection for doubly transformed BL21-Gold (DE3) was performed by growth in LB-media containing kan and amp. Expression and purification of the hybrid tetramers was performed as described (*10*). (**A**) Preparative anion exchange chromatography of the hybrid tetramers reveals that they can be separated. The elution time of tetramers **1** through **5** increased in proportion to the number of $FT_2$-T119M subunits composing the tetramer, from 0 to 4 subunits, respectively. (**B**) Verification of tetramer subunit composition was performed by RP-HPLC/electrospray ionization mass spectrometry (ESI-MS) under acidic conditions (1% trifluoroacetic acid) using a $CH_3CN$ elution gradient that denatures the hybrid tetramers into unfolded subunits, the elution time being shorter for the $FT_2$-T119M (peak A) relative to V30M subunits (peak B) due to their increased polarity.

Little is known about the distribution of tetramers **1** to **5** in compound heterozygotes because of our inability to separate them under nondenaturing conditions. Expression levels and kinetics of folding, degradation, and subunit exchange as well as thermodynamic differences among tetramers **1** to **5** contribute to the observed distribution. The propensity of V30M and T119M subunits to form hybrid tetramers is high, as demonstrated by the distribution revealed by coexpression of these proteins in *E. coli* (Fig. 1A; favoring T119M-rich tetramers) and the near-statistical distribution of tetramers arising from in vitro reconstitution of equimolar unfolded subunits (Fig. 4E) (*10*). T119M suppression requiring hybrid tetramer formation appears similar in vitro and in vivo, on the basis of suppression of amyloidogenicity and the benign disease phenotype, respectively (*4, 5*). We presume that the reason pathology is observed at all in compound heterozygotes is due to the low concentration of amyloidogenic tetramer **1** and modestly amyloidogenic tetramer **2** which can form fibrils, unlike tetramers **3**, **4**, and **5**. To explain the tissue-specific deposition of V30M TTR and the bias toward fibrils rich in V30M subunits (*21–23*), we propose that a given tissue imposes a denaturation stress of fixed magnitude that can only utilize the less stable tetramers as amyloid precursors (e.g., **1** and to a lesser extent **2**) (*24*). Both heterozygotes (aggressive disease phenotype) and compound heterozygotes have comparable amounts of V30M TTR subunits, yet the latter exhibit a benign disease phenotype (*4, 5*). Thus, it is very unlikely that the V30M TTR subunit causes the disease by a mechanism associated with its normal fold. The dramatic reduction in amyloidogenicity (in vitro) of tetramers mimicking those found in compound heterozygotes supports the amyloid hypothesis origin of FAP.

V30M FAP is now treated by liver transplantation, replacing V30M TTR with WT TTR, resulting in the clearance of amyloid and a dramatic health improvement—further supporting the amyloid hypothesis (*25*). The predictions made by the data outlined above, if confirmed in vivo, suggest that a gene therapy approach for the synthesis of the T119M *trans*-suppressor subunits in the liver is likely to inhibit TTR amyloid formation. Administration of T119M subunits that could be incorporated into TTR tetramers after secretion represents an alternative strategy (Fig. 4D) (*26*).

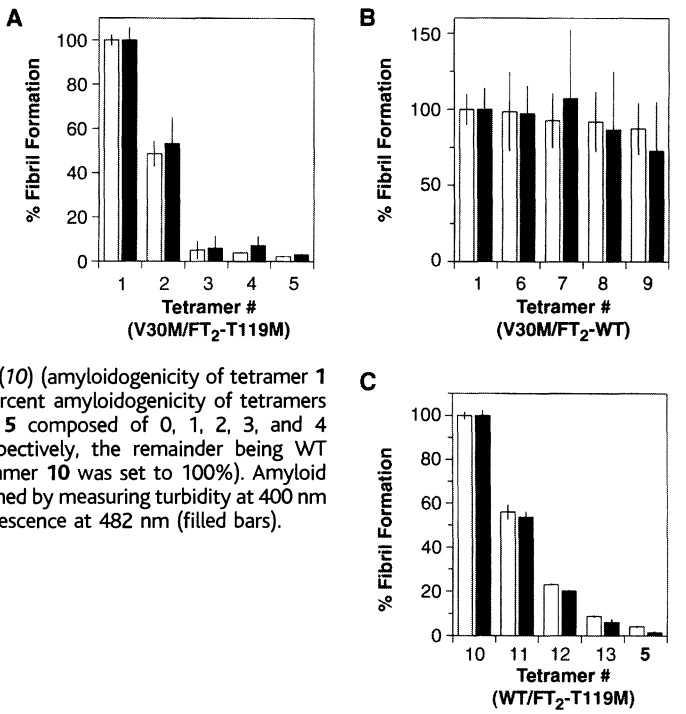


**Fig. 2.** Amyloidogenicity of tetramers with defined subunit composition. The percent amyloidogenicity of (**A**) tetramers **1** to **5** composed of 0, 1, 2, 3, and 4 $FT_2$-T119M subunits and (**B**) tetramer **1** and tetramers **6** to **9** composed of 0, 1, 2, 3, and 4 $FT_2$-WT subunits, respectively (the remainder being V30M) were evaluated at pH 4.4 after 72 hours as described (*10*) (amyloidogenicity of tetramer **1** was set to 100%). (**C**) Percent amyloidogenicity of tetramers **10** to **13** and tetramer **5** composed of 0, 1, 2, 3, and 4 $FT_2$-T119M subunits, respectively, the remainder being WT (amyloidogenicity of tetramer **10** was set to 100%). Amyloid quantification was performed by measuring turbidity at 400 nm (open bars) and ThT fluorescence at 482 nm (filled bars).

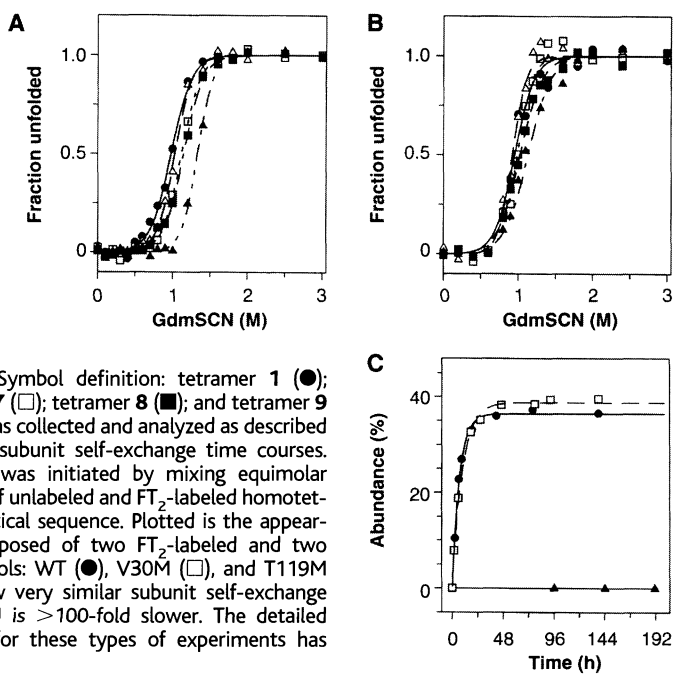


**Fig. 3.** Stability of hybrid tetramers and TTR homotetramer subunit exchange kinetics. (**A**) Guanidinium thiocyanate (GdmSCN) denaturation curves of tetramers **1** to **5**. Symbol definition: tetramer **1** (●); tetramer **2** (△); tetramer **3** (□); tetramer **4** (■); and tetramer **5** (▲). (**B**) GdmSCN denaturation curves of tetramer **1** and tetramers **6** to **9**. Symbol definition: tetramer **1** (●); tetramer **6** (△); tetramer **7** (□); tetramer **8** (■); and tetramer **9** (▲). The unfolding data was collected and analyzed as described (*28*). (**C**) Homotetramer subunit self-exchange time courses. Subunit exchange (4°C) was initiated by mixing equimolar concentrations (1.8 μM) of unlabeled and $FT_2$-labeled homotetramers of otherwise identical sequence. Plotted is the appearance of a tetramer composed of two $FT_2$-labeled and two unlabeled subunits. Symbols: WT (●), V30M (□), and T119M (▲). V30M and WT show very similar subunit self-exchange kinetics, however, T119M is >100-fold slower. The detailed experimental procedure for these types of experiments has been reported (*11*).

### References and Notes


1. J. W. Kelly, *Curr. Opin. Struct. Biol.* **6**, 11 (1996).
2. C. M. Dobson, *Trends Biochem. Sci.* **24**, 329 (1999).
3. A. L. Fink, *Folding Des.* **3**, 9 (1998).
4. T. Coelho *et al.*, *J. Rheumatol.* **20**, 179 (1993).
5. T. Coelho *et al.*, *Neuromuscular Disord.* **6**, 27 (1996).
6. S. L. McCutchen, Z. Lai, G. J. Miroy, J. W. Kelly, W. Colon, *Biochemistry* **34**, 13527 (1995).
7. I. L. Alves, M. T. Hays, M. J. M. Saraiva, *Eur. J. Biochem.* **249**, 662 (1997).
8. M. P. Sebastiao, V. Lamzin, M. J. Saraiva, A. M. Damas, *J. Mol. Biol.* **306**, 733 (2001).
9. Single-letter abbreviations for the amino acid residues are as follows: D, Asp; K, Lys; M, Met; T, Thr; V, Val; and Y, Tyr.
10. See supplemental Web information available at www.sciencemag.org/cgi/content/full/293/5539/2459/DC1.
11. F. Schneider, P. Hammarström, J. W. Kelly, *Protein Sci.* **10**, 1606 (2001).
12. P. Hammarström, X. Jiang, S. Deechongkit, J. W. Kelly, *Biochemistry*, **40**, 11453 (2001).
13. M. M. Santoro, D. W. Bolen, *Biochemistry* **27**, 8063 (1988).
14. B. Schuler, R. Seckler, *J. Mol. Biol.* **281**, 227 (1998).
15. P. V. Nikolova, K.-B. Wong, B. DeDecker, J. Henckel, A. R. Fersht, *EMBO J.* **19**, 377 (2000).
16. G. Holmgren *et al.*, *Clin. Genet.* **34**, 333 (1988).
17. G. Holmgren *et al.*, *Clin. Genet.* **41**, 39 (1992).
18. O. Sandgren, G. Holmgren, E. Lundgren, *Arch. Ophthalmol.* **108**, 1584 (1990).
19. S. Ikeda, T. Nakano, N. Yanagisawa, M. Nakazato, H. Tsukagoshi, *Eur. Neurol.* **32**, 308 (1992).
20. Subunit exchange: Incubation of V30M and $FT_2$-T119M or T119M was performed to produce hybrid tetramers by subunit exchange. Equimolar amounts of $FT_2$-T119M or T119M and V30M (0.2 mg/ml) were incubated in 25 mM Tris-HCl (pH 7.4) for 18 days at 4°C. Hybrid formation was verified by analytical ion exchange chromatography. After 18 days, only 20% of the homotetramers had exchanged and the mixture exhibiting the expected extent of fibril formation (80%). Co-reconstituted TTR: Formation of hybrid tetramers by in vitro refolding/tetramer reconstitution was performed by

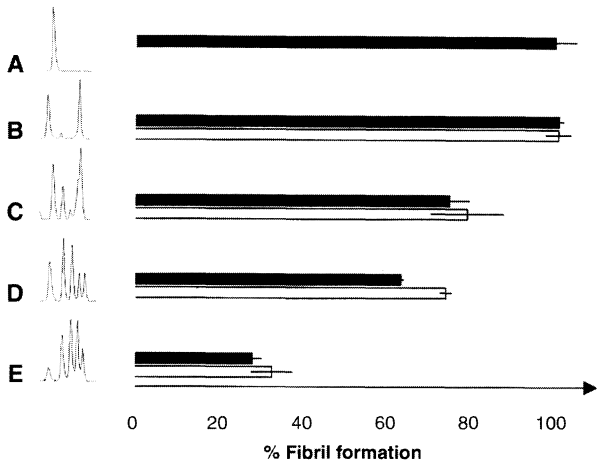


**Fig. 4.** Fibril formation as a function of the extent of hybrid tetramer formation. Chromatograms from analytical anion exchange chromatography quantifying the amount of subunit exchange are shown on the left and the extent of fibril formation represented by bar graphs (turbidity at 400 nm) on the right. (**A**) The extent of amyloidogenicity from the V30M homotetramer **1** [0.2 mg/ml (pH 4.4); 37 °C; 72 hours; set to 100%]. Entry (**B**) displays the amyloidogenicity arising from mixing homotetramers **1** and **5** (open bar) and **1** (filled bar) with an untagged T119M homotetramer immediately before triggering fibril formation by lowering the pH. No suppression of V30M amyloidogenicity occurs, due to lack of subunit exchange. (**C**) When tetramer **1** and the T119M homotetramer (filled bar) or tetramers **1** and **5** (open bar) are preincubated at 4°C for 18 days (*20*) some exchange occurs, consistent with the modest suppression of amyloidogenicity. (**D**) The unfolding/refolding protocol (*26*) provides assembly-competent monomeric T119M suppressor subunits which exchange with subunits in V30M homotetramer **1** after 24 hours (4°C). The amyloidogenicity of the tetramers resulting from exchange between native V30M and monomeric T119M (filled bar) or $FT_2$-T119M (open bar) is shown. (**E**) Amyloid formation from co-reconstituted TTR [V30M and T119M (filled bar) or $FT_2$-T119M (open bar)] as described in (*20*), affording a near-statistical distribution of tetramers (1:4:6:4:1), exhibited a 70% inhibition of amyloid formation.

rapid dilution of equimolar concentrations (to 0.05 mg/ml) of unfolded V30M and $FT_2$-T119M or T119M subunits (in 6.5 M GdmCl preincubated for 48 hours at 4°C) at 25°C. The refolded protein was purified by dialysis and gel filtration (Superdex 75, Pharmacia).

21. F. E. Dwulet, M. D. Benson, *Proc. Natl. Acad. Sci. U.S.A.* **81**, 694 (1984).
22. M. J. M. Saraiva, S. Birken, P. P. Costa, D. S. Goodman, *J. Clin. Invest.* **74**, 104 (1984).
23. Y. Ando *et al.*, *Amyloid* **6**, 119 (1999).
24. By extension, the impotency of the WT subunit as a suppressor predicts that the fibrils in heterozygous patients (V30M/WT) formed in tissues imposing a strong denaturation stress will be composed of both V30M and WT subunits, because all five tetramers would be amyloidogenic. The 1:1 ratio of V30M and WT subunits composing cardiac amyloid deposits seems to verify this prediction (*27*). In other tissues, however, such as in the kidney (*21, 22*) and the vitreous body (*23*), the bias toward V30M subunits composing the deposits is evident, suggesting that the denaturation stress in these tissues is not as severe; therefore, only tetramer **1** and V30M-rich tetramers **6** and **7** serve as precursors as opposed to the WT-rich tetramers **8** and **9**, which are more stable, at least toward chaotrope denaturation (Fig. 3B) (*10*).
25. O. B. Suhr *et al.*, *Transplantation* **60**, 933 (1995).
26. Proof of principle that it is possible to include T119M supressor subunits into a TTR tetramer after secretion was demonstrated by adding folded T119M monomers to V30M homotetramer **1** undergoing subunit exchange at 4°C. A folded T119M or $FT_2$-T119M monomer was produced by first unfolding the tetramer in 6.5 M guanidinium chloride (GdmCl) at 4°C (48 hours) and then refolding it by rapid dilution. The monomer resists self-tetramerization at 4°C, allowing it to be mixed with tetramer **1** (4°C), which by subunit exchange incorporates T119M subunits and resists acid-induced fibril formation (Fig. 4D). A detailed procedure is available (*10*). Further elaboration will be required to achieve this result by intravenous administration of T119M TTR monomers.
27. M. Yazaki *et al.*, *Biochem. Biophys. Res. Commun.* **274**, 702 (2000).
28. TTR (1 μM monomer concentration) was prepared in GdmSCN (0 to 3 M) and incubated for 24 hours (25°C) in buffer [50 mM phosphate buffer (pH 7.0) with 1 mM EDTA and 1 mM dithiothreitol added]. Denaturation curves were generated by the ratio of the tryptophan fluorescence intensity [355 nm (unfolded maximum)]/[335 nm (folded maximum)]; excitation is at 295 nm. The unfolding data were normalized from linear baseline dependence on denaturant and fitted to a two-state unfolding transition as described (*13*). Estimates of $\Delta G_{NU} = -RT\ln [D]/[N]$ were calculated assuming a linear dependence of $\Delta G$ on denaturant concentration using $\Delta G_{NU} = \Delta G_{NU}{}^{H_2O} - m[GdmSCN]$.
29. We thank G. Dendle for help with protein expression and purification, H. Purkey for assistance with the T4 binding assay, J. White for RBP binding measurements, S. Deechongkit and H. M. Petrassi for help with analytical ultracentrifugation, and A. Sawkar for assistance with the unfolding refolding protocol. We are also grateful to J. Buxbaum for fruitful discussions regarding the clinical aspects and R. Lerner for critical comments on the manuscript. Supported by a grant from NIH (DK46335-09), The Skaggs Institute of Chemical Biology, The Lita Annenberg Hazen Foundation, and a postdoctoral fellowship to P.H. from The Wenner-Gren Foundations.

3 May 2001; accepted 3 August 2001

# Strand-Specific Postreplicative Processing of Mammalian Telomeres

**S. M. Bailey,[1] M. N. Cornforth,[2] A. Kurimasa,[3] D. J. Chen,[3] E. H. Goodwin[1]***

**Telomeres are specialized nucleoprotein structures that stabilize the ends of linear eukaryotic chromosomes. In mammalian cells, abrogation of telomeric repeat binding factor TRF2 or DNA-dependent protein kinase (DNA-PK) activity causes end-to-end chromosomal fusion, thus establishing an essential role for these proteins in telomere function. Here we show that TRF2-mediated end-capping occurs after telomere replication. The postreplicative requirement for TRF2 and DNA-PKcs, the catalytic subunit of DNA-PK, is confined to only half of the telomeres, namely, those that were produced by leading-strand DNA synthesis. These results demonstrate a crucial difference in postreplicative processing of telomeres that is linked to their mode of replication.**

Telomeres are nucleoprotein structures at the ends of chromosomes that are composed of repetitive G-rich sequence (TTAGGG in vertebrates) and a variety of associated telomeric binding proteins. Together, they form a dynamic terminal structure that "caps" the natural ends of linear chromosomes (*1*, *2*). This cap prevents degradation of chromosome ends and protects against inappropriate recombination. TRF2 (*3*, *4*) and the three subunits of DNA-PK—Ku70, Ku80, and the catalytic subunit DNA-PKcs (*5*–*8*)—are among the proteins that participate directly in capping mammalian chromosomes. Direct visualization of mammalian telomeres by electron microscopy has revealed the existence of terminal structures known as t loops (*9*), which are created when a telomere end loops back on itself and invades an interior segment of duplex telomeric DNA. By sequestering natural chromosome ends, t loops may render telomeres nonrecombinogenic. It has been proposed that formation of t loops is mediated by TRF1 and TRF2 and requires a single-stranded extension of the TTAGGG sequence

[1]Bioscience Division, Los Alamos National Laboratory, Los Alamos, NM 87544, USA. [2]Department of Radiation Oncology, University of Texas Medical Branch, Galveston, TX 77550, USA. [3]Cell and Molecular Biology Division, Lawrence Berkeley National Laboratory, Berkeley, CA 94720, USA.

*To whom correspondence should be addressed. E-mail: egoodwin@telomere.lanl.gov